Polymer 50 (2009) 2856–2862

Contents lists available at ScienceDirect

Polymer

journal homepage: www.elsevier.com/locate/polymer

Effect of the addition of hydrophobic clay on the electrochemical property of polyacrylonitrile/$LiClO_4$ polymer electrolytes for lithium battery

Y.W. Chen-Yang [a,*], Y.T. Chen [a], H.C. Chen [b], W.T. Lin [b], C.H. Tsai [a]

[a] Department of Chemistry and Center for Nanotechnology, Chung Yuan Christian University, 200 Chung-Pei Road, Chung-Li, Taoyuan County 32023, Taiwan, ROC
[b] Taiwan Textile Research Institute, Taipei County 23674, Taiwan, ROC

ARTICLE INFO

Article history:
Received 5 September 2008
Received in revised form
19 January 2009
Accepted 2 April 2009
Available online 23 April 2009

Keywords:
Composite polymer electrolyte
Montmorillonite
Lithium battery

ABSTRACT

In this study, an organoclay, ALA–MMT, was prepared by the ionic exchange reaction of montmorillonite (MMT) with 12-aminododecanoic acid (ALA). ALA–MMT was then used as a filler to prepare a series of composite polymer electrolytes based on polyacrylonitrile (PAN) and $LiClO_4$. The effect of the addition of ALA–MMT on the properties of the composite polymer electrolytes (CPEs) was investigated by XRD, FT-IR, DSC, tensile strength, AC impedance, and cyclic voltammetry measurements. It was found that the ALA–MMT particles were well dispersed in the CPEs. Owing to the incorporation of ALA–MMT, a higher fraction of the free anions was obtained, indicating that the lithium salt dissolved in the PAN matrix more effectively for the CPE than in the PAN/$LiClO_4$ polymer electrolyte. Moreover, the glass-transition temperature was reduced, benefiting the ion transport. The best ionic conductivity at room temperature was obtained from the CPE with 7 wt% of the modified clay and 0.6 M $LiClO_4$ per PAN repeat unit (CPE-7) and was more than seven times higher than that from the corresponding PAN/$LiClO_4$ polymer electrolyte (CPE-0). The mechanical property and the cation transference number, t_+, of CPE-7 are largely increased compared to that of CPE-0. Besides, the CPEs were electrochemically stabilized up to 4.75 V and the corresponding cell exhibited excellent electrochemical stability and cyclability over the potential range between 0 V and 4.0 V vs. Li/Li^+.

1. Introduction

The preparation of ion-conducting solid polymer electrolyte membranes has received considerable attention. Since the solid polymer electrolytes are used as both an electrolyte and a separator, they have to meet not only such requirements as high ionic conductivity, wide electrochemical stability window, easy processability, and light weight, but also acceptable thermal and mechanical performances [1–4]. However, most of the polymer electrolytes reported had several disadvantages, which limit their commercial applications. One major drawback is their relatively low ionic conductivity at ambient temperature. Various methods have been applied to increase their ionic conductivity [5]. One of the most successful approaches to improve it is to prepare the composite polymer electrolyte (CPE) by the addition of inorganic fillers, such as ceramic powders [3,6–9], natural materials [3,10–17], and mesoporous materials [18–23].

Mineral clay is a special type of natural materials that is composed of two fused silica tetrahedral sheets sandwiching an edge-shared octahedral sheet of either magnesium or aluminum hydroxide. Because of its interesting properties, such as ion exchangeability, thermal stability, and intercalation/exfoliation possibility of the silicate layers, the preparation and characterization of polymer/clay nanocomposites comprising the inorganic nanolayers of the mineral clay and organic polymer have been actively studied [3,10–17,24,25]. These reports showed that the addition of the nanolayers of mineral clay in the polymer electrolyte could not only increase ionic conductivity, thermal stability, and mechanical strength [12,13], but could also enhance the electrochemical stability and cationic transfer number of the polymer electrolytes [3].

Polyacrylonitrile (PAN) is one of the popular polymers used as gel-type polymer electrolytes for lithium batteries, which generally exhibit about 10^{-3} S/cm of the ionic conductivities [1]. Nevertheless, the poor dimensional stability, the possible hazard owing to the presence of the massive organic solvent incorporated, and a progressive evaporation of the liquid solvent that may induce a progressive decrease in the ionic conductivity limit the practical application of gel-type polymer electrolytes. To minimize these

* Corresponding author. Tel.: +886 3 2653317; fax: +886 3 2653399.
E-mail address: yuiwhei@cycu.edu.tw (Y.W. Chen-Yang).

0032-3861/$ – see front matter © 2009 Elsevier Ltd. All rights reserved.
doi:10.1016/j.polymer.2009.04.023

disadvantages, the preparation and properties of the PAN-based solid polymer electrolytes have been reported [10,26]. The results showed that the addition of α-Al_2O_3 into the PAN/$LiClO_4$ electrolyte improved the properties of the corresponding polymer electrolyte, such as ionic conductivity, mechanical property, and the cation transference number. Chang and Chen [10] prepared an organo-clay-containing PAN/$LiCF_3SO_3$-based solid polymer electrolyte; however, its conductivity was only 10^{-5} S/cm, which was far below 10^{-4} S/cm, the limit value for practical use in battery. Therefore, finding a better organoclay for the preparation of PAN-based composite polymer electrolyte is still an attractive topic.

Unlike the phenyl-terminal alkyl ammonium salt reported [10], in this study, the hydrophobic clay, ALA–MMT, was prepared by the ionic exchange reaction of MMT with a carboxy-terminal alkyl ammonium salt (ALA salt). The as-prepared ALA–MMT was used as a filler to prepare a series of PAN-based CPEs with $LiClO_4$ and was anticipated to have better dispersion in the polymer matrix owing to the presence of the carboxy groups. The ionic conductivity, thermal property, mechanical property, and electrochemical property of the CPEs have been investigated.

2. Experiment

2.1. Material

Polyacrylonitrile (PAN, M_w: 150,000, sp^2), lithium perchlorate ($LiClO_4$) (reagent grade), and dimethylformamide (DMF) were purchased from Aldrich. $LiClO_4$ was dried under vacuum ($<10^{-3}$ Torr) for 24 h at 140 °C before use. The montmorillonite clays (PK805) were supplied by Paikong Ceramic Materials Co., Taiwan.

2.2. Preparation of the composite polymer electrolytes (CPEs) and composite polymer (CP)

To prepare the PAN/$LiClO_4$/ALA–MMT [27] composite polymer electrolyte (CPE), 0.2 g of PAN was first dissolved with a small amount of DMF. Then, 0.241 g of lithium salt, $LiClO_4$, was added, and the solution was well stirred. A designated amount of ALA–MMT was then added and the PAN/$LiClO_4$/ALA–MMT solution was further sonicated for 15 min using an ultrasound bath by Delta D200H to disperse the ALA–MMT particles. The solution was later cast on a flat glass slide and dried in a vacuum oven at 80 °C for at least 24 h to remove the solvent. The average thickness of the polymer electrolyte membranes was about 150 μm. In the rest of this study, CPE-x is used as the abbreviation of the polymer electrolyte sample containing x wt% of ALA–MMT. For comparison, a corresponding composite polymer without $LiClO_4$ (PAN/MMT, PAN/ALA–MMT) was also prepared using the same method. The compositions and the abbreviations of CPEs and CPs are listed in Table 1.

Table 1
Compositions and abbreviations of the composites.

	PAN (g)	$LiClO_4$ (g)	ALA–MMT (wt%)	MMT (wt%)
CPE-0	0.20	0.241	0	0
CPE-1	0.20	0.241	1	0
CPE-3	0.20	0.241	3	0
CPE-5	0.20	0.241	5	0
CPE-7	0.20	0.241	7	0
CPE-8	0.20	0.241	8	0
CP-7-AM	0.20	0	7	0
CP-7-M	0.20	0	0	7

2.3. Instruments

2.3.1. WXRD analysis

X-ray diffraction (XRD) study of the samples was performed on a Rigaku D/MAX-3C OD-2988N X-ray diffractometer (35 kV, 25 mA) with a copper target ($\lambda = 1.5405$ Å) and Ni filter at a scanning rate of 4°/min from 2° to 10°.

2.3.2. Ionic conductivity

The ionic conductivities of the polymer electrolytes were measured by the AC impedance method in the temperature ranging from 30 °C to 80 °C. The samples were sandwiched between stainless steel blocking electrodes and placed in a temperature-controlled oven at vacuum ($<10^{-2}$ Torr) for 2 h before measurement. The experiments were performed in a constant area cylindrical cell of an electrode diameter of 1.76 cm^2. The impedance measurements were carried out on a computer interfaced with an HP 4192A impedance analyzer over the frequency range of 5 Hz to 13 MHz.

2.3.3. Differential scanning calorimetry

Thermal analysis was carried out on a Differential scanning calorimetry (DSC) instrument from Seiko (DSC-220C) with a scan rate of 10 °C/min ranging from −150 °C to 150 °C. Approximately 5–10 mg of each sample was weighted and sealed in an aluminum pan for the analysis.

2.3.4. Infrared spectroscopy

The conventional KBr disk method was employed to measure the infrared spectra of the composite films. The solution was cast onto a KBr disk and the solvent was removed under vacuum at 80 °C for 24 h and then stored in the dry box for 2 h before measurement. The Fourier transformation Infrared spectroscopy (FT-IR) spectra were recorded on a Bio-Rad FTS-7 with a wave number resolution of 2 cm^{-1}.

2.3.5. Morphology property

The fractured surface morphologies of the nanocomposites were examined using a field emission scanning electron microscopy (JEM-6300) instrument. The specimens were slightly cracked with a thin razor blade and then fractured with a hammer. Before examination, all the samples were adhered onto the adhesive carbon tapes supported by a circular metallic disk. The samples were coated with platinum using a sputter coater to avoid charging.

2.3.6. Mechanical property

The mechanical properties were measured using a tensile tester (Q-test) equipped with a 100-N load cell and interfaced with a computer for data collection. For the measurement, the sample with the dimension of 50 × 6 mm^2 was pulled at a constant rate of 2 inch/min.

2.3.7. Electrochemical property

The electrochemical properties of the as-prepared composite polymer electrolyte films were studied by the linear sweep voltammetry and cyclic voltammetry measurements on a three-electrode cell, in which a Pt plate was employed as the working electrode, and lithium metal served as the counter and reference electrodes. The assembly was put in a dry box filled with argon gas. The linear sweep was run from 2.5 V to 6.0 V (vs. Li/Li^+) and the cyclic voltammetry potential range was 0–4 V (vs. Li/Li^+) at a scan rate of 10 mV/s.

2.3.8. Lithium ion transference numbers

The lithium ion transference number (t_+) was measured using the technique reported [28,29]. The technique consisted of the measurement of the initial lithium interfacial resistance (R_0) with

impedance spectroscopy in the frequency range of 1 MHzto5 Hz, the application of a small voltage (0.1 V) until a steady current was obtained (I_s), and the measurement of the final interfacial resistance (R_f) in the same frequency range. The electrochemical cell consisted of a rectangular piece of polymer electrolyte sandwiched between two lithium foils. The electrolyte was sandwiched between two lithium-unblocking electrodes to form a symmetrical Li/electrolyte/Li cell used for the t_+ test. The cell was assembled and sealed in an argon-filled UNILAB glove-box. The impedance of the cell was measured using an Autolab PGSTAT 30 potentiostat/galvanostat analyzer between the frequencies of 5 Hz and 1 MHz. The measurements were performed using a Solartron 1260 impedance/gain-phase analyzer coupled with a Solartron 1287 electrochemical interface.

3. Results and discussion

3.1. WXRD analysis

The montmorillonite used in this study was a clay containing stacked silicate sheets ~10 Å in thickness and ~2180 Å in length with Cation Exchange Capacity (CEC) = 98 meq/100 g and was made organophilic through an ion exchange reaction by reacting with the quaternary ammonium salt of ALA, which contains a 12 carbon-long alkyl acidic group. It is anticipated that the long alkyl group of the quaternary ammonium would intercalate in the MMT clay galleries and enlarge the distance between the layers. To confirm this, the interlayer spacing of the clays was determined from the XRD peak using the Bragg equation:

$$n\lambda = 2d \sin\theta$$

where d corresponds to the spacing between the diffraction lattice planes, θ is the diffraction angle, and λ is the wavelength of the X-ray (1.5405 Å). Fig. 1 displays the XRD patterns of MMT, ALA–MMT, CP-7-M, the PAN/MMT (7 wt%) composite, CP-7-AM, the PAN/ALA–MMT (7 wt%) composite, and CPE-7. It is found that after modification, the basal interlayer spacing of the silicate layers calculated from the θ value of (1,0,0) increased from 1.2 nm to 1.4 nm, confirming that the long alkyl group intercalates into the silicate galleries (Fig. 1(a) and (b)). As indicated in Fig. 1(c), the basal interlayer spacing of CP-7-M is about 1.8 nm, indicating that the PAN polymer chains could intercalate in the silicate layer gallery and further expanded the interlayer spacing within MMT. Nevertheless, Fig. 1(d) shows that the (1,0,0) peak of CP-7-AM

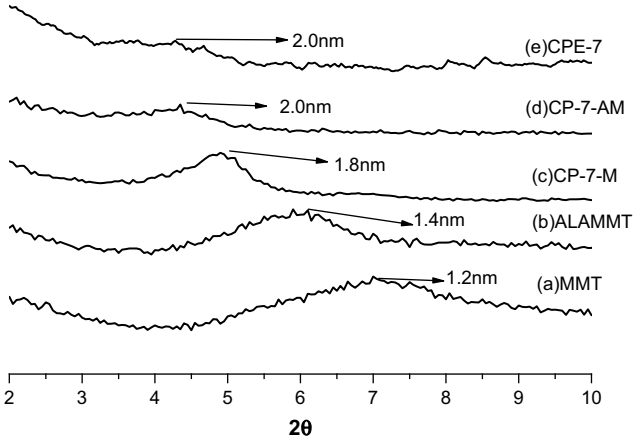

Fig. 1. X-ray diffraction patterns of (a) MMT (b) ALA–MMT (c) CP-7-M (d) CP-7-AM (e) CPE-7.

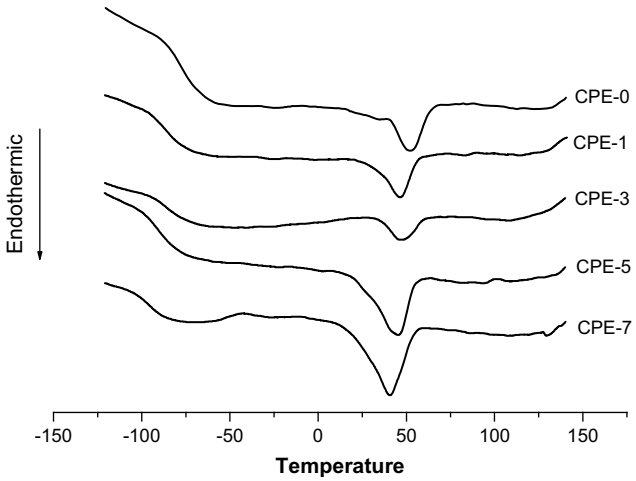

Fig. 2. DSC thermograms of CPE-x.

shifted to a lower angle, corresponding to 2.0 nm and is broader than that of CP-7-M. This indicates that part of the layer-structure crystals was destroyed and the basal interlayer spacing was expanded more in CP-7-AM than in CP-7-M. The increase of the interlayer spacing in CP-7-AM implies that the PAN polymer chains intercalated more in the silicate layer gallery within ALA–MMT. This also suggests that ALA–MMT had better compatibility with PAN matrix than the unmodified MMT, which is attributed to the presence of the long alkyl carboxy group of ALA. Besides, the 2θ value of CPE-7 shown in Fig. 1(e) is similar to that of CP-7-AM in Fig. 1(d), indicating that the presence of the lithium salt did not affect the interlayer spacing of the ALA–MMT in the composite.

3.2. Thermal analysis

The thermal properties of the as-prepared CPEs were studied by DSC measurement. As shown in Fig. 2 and Table 2, when the ALA–MMT content was increased to 7 wt%, the glass-transition temperature (T_g) and the melting point (T_m) of the polymer electrolyte were decreased from about −78 °C and 53 °C to −94 °C and 40 °C, respectively. The result implies that the flexibility of the PAN polymer chain was increased by increasing the ALA–MMT content. This may be attributed to the reduction of the interaction between Li^+ and the C≡N groups of PAN matrix, which will be discussed by the FT-IR spectra in the following section. The decrease of T_g in turn may assist to enhance the ionic conductivity.

3.3. FT-IR spectroscopy

The FT-IR spectroscopy was used for probing the microscopic details of the CPEs and was anticipated to provide the information on the interactions among PAN, $LiClO_4$, and ALA–MMT. The previous publications [30–33] reported that the change in the absorbance of ClO_4^- that appeared between 600 and 650 cm^{-1} reveals the

Table 2
DSC thermal data and ionic conductivities of CPE-x.

	T_g (°C)	T_m (°C)	σ at 30 °C (S cm^{-1})	E_a (kJ mol^{-1})
CPE-0	−78	53	0.34×10^{-4}	9.5
CPE-1	−85	49	1.31×10^{-4}	10.0
CPE-3	−87	47	1.72×10^{-4}	13.3
CPE-5	−90	45	1.97×10^{-4}	16.3
CPE-7	−94	40	2.44×10^{-4}	16.7

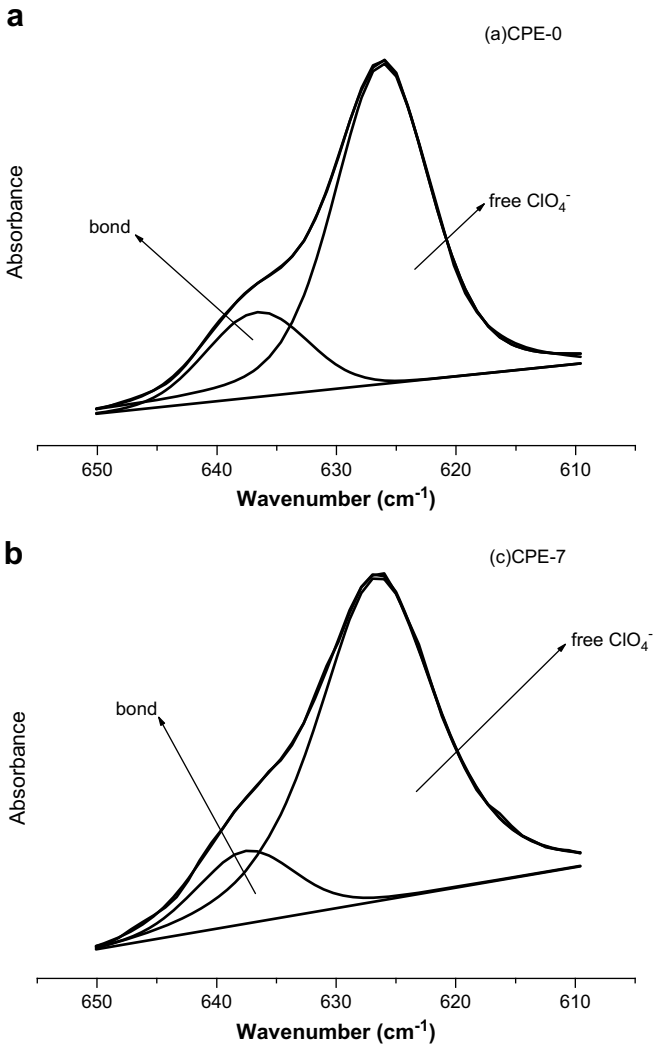

Fig. 3. Peak fitting of the ClO_4^- absorbance for (a) CPE-0 and (b) CPE-7.

dissociation of $LiClO_4^-$. The absorbance was deconvoluted into two contributions: the one observed at ~624 cm^{-1} was assigned to the "free" anion, which does not interact directly with the lithium cation, and the other at ~635 cm^{-1} was attributed to the contacted ion pair. Accordingly, the curve fitting of a Gaussian–Lorentzian peak to the ClO_4^- absorbance region for CPE-0 and CPE-7 was applied and is shown in Fig. 3. The corresponding peak area ratios of the vibration peaks deconvoluted are summarized in Table 3. As listed, the fraction of the free ClO_4^- of CPE-5 dramatically increased from that of CPE-3, while it increased slowly with the increase in the

Table 3
FT-IR peak positions and percentage of free ClO_4^- for CPE-x.

Sample	Free ClO_4^-		Bonded ClO_4^-	
	(cm^{-1})	(%)[a]	(cm^{-1})	(%)
CPE-0	626	80.2	636	19.8
CPE-1	626	80.4	637	19.6
CPE-3	626	81.6	636	18.4
CPE-5	626	88.2	637	11.8
CPE-7	626	90.0	637	10.0
CPE-8	626	87.9	637	12.1

[a] The percentage of the free ClO_4^- measured from the area ratio of the deconvoluted ClO_4^- peaks.

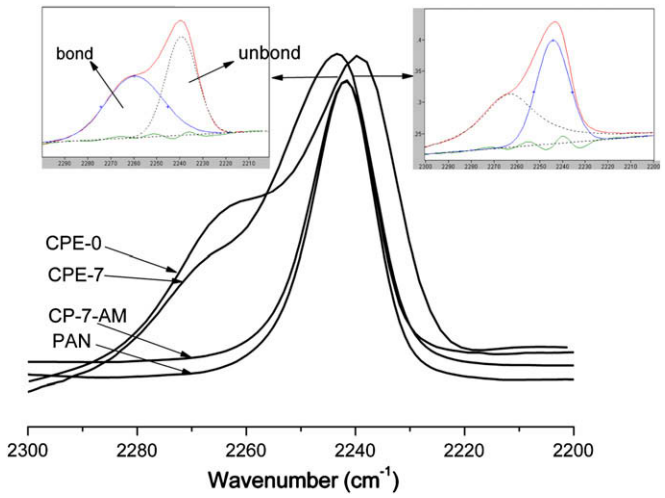

Fig. 4. FT-IR spectra of the C≡N absorbance for PAN, CP-7-AM, CPE-0, CPE-7, and peak fitting of the C≡N absorbance for CPE-0 and CPE-7.

ALA–MMT concentration in the low clay concentration range (≤3 wt%), implying that the dissolution of the $Li^+ClO_4^-$ salt was effectively increased when enough ALA–MMT (≥5 wt%) particles were dispersed in the electrolytes. This is attributed to the fact that the Li^+ ion was separated from its counter ion, ClO_4^-, when enough interactions among the lithium ion and the clay layers were present [10]. Besides, the increase of the $Li^+ClO_4^-$ dissolution resulted in an increase of the charge carriers that would enhance the ionic conductivity of the CPE composites. Nevertheless, as the ALA–MMT loading exceeded 7 wt%, the fraction of the free anions for the CPE decreased. This is attributed to the aggregation of the highly loaded organoclay particles, which reduced the surface area, resulting in the reduction of its influence on the salt dissociation.

On the other hand, because the structure of PAN involves only the simple C–C backbone and the C≡N side groups, the change in the C≡N vibration absorbance caused by the presence of the salt and/or the filler can provide an important information regarding the change in the interactions related to the polymer-side chain in the CPE. Fig. 4 shows the FT-IR spectra of the C≡N vibration absorbance of PAN, CP-7, CPE-0, and CPE-7 between 2200 and 2300 cm^{-1}. According to the previous report [34], the absorbance was also deconvoluted into two contributions, the unbonded C≡N between 2235 and 2250 cm^{-1}, and the bonded C≡N between 2255 and 2270 cm^{-1}, for the CPEs and shown in Fig. 4 for CPE-0 and CPE-7. As shown in Table 4, the percentage of the bonded C≡N groups decreased with the ALA–MMT content, implying that the interaction between the Li^+ ion and C≡N, the bonded C≡N, decreased because of the presence of ALA–MMT. This also suggests that the Li^+ ions might interact with the clay [8], providing the hopping sites for Li^+ ions to migrate into the CPEs, resulting in an enhancement of the ionic conductivity as discussed below. This result is similar to the result obtained in the Al_2O_3-containing PAN/

Table 4
FT-IR peak positions and percentage of C≡N for CPE-x.

Sample	Unbounded C≡N		Bonded C≡N	
	(cm^{-1})	(%)	(cm^{-1})	(%)
CPE-0	2239	42.7	2258	57.3
CPE-1	2240	54.1	2262	51.9
CPE-3	2238	56.4	2261	43.6
CPE-5	2239	60.6	2263	39.4
CPE-7	2240	66.0	2266	34.0

$LiClO_4$ CPEs [27]. Furthermore, it is also seen that the absorption peak of the CN for CP-7 was almost the same as that for the pure PAN membrane. This implies that with the addition of 7 wt% of the ALA–MMT, the CN vibration mode remains unchanged. In other words, no significant interaction between the CN groups and the ALA–MMT is found in CP-7. Thus, the results indicate that the interaction between Li^+ and CN was interrupted by the dispersed ALA–MMT particles in CPEs and the solvation of the $LiClO_4$ salt was increased.

3.4. Ionic conductivity

Generally, the ionic conductivity of an electrolyte, σ, relates to the number of the charge carriers and their mobility in the electrolyte is often defined as follows:

$$\sigma = \sum n_i z_i \mu_i$$

where n_i, z_i, and μ_i refer to the number of charge carriers, the ionic charge, and the ionic mobility, respectively. The ionic conductivities of the as-prepared CPEs measured by the AC impedance measurement at 30 °C vs. the ALA–MMT content are shown in Fig. 5. It shows that the ionic conductivity of the PAN-based electrolytes without ALA–MMT (CPE-0) was 3.4×10^{-5} S/cm. The conductivity increased continuously with the increase of the ALA–MMT content up to 7 wt%. This is attributed to the increase of the n_i value, which is due to the increase of the dissociation of the lithium salt, and the increase of mobility of the Li^+ caused by the reduction of the coordination with the C≡N group as indicated by the FT-IR result. The maximum value of conductivity obtained from CPE-7 was 2.44×10^{-4} S/cm, which was more than seven times higher than that obtained from CPE-0 and corresponded to the highest dissociation of the salt in the system. Besides, when the ALA–MMT content increased to 8 wt%, the conductivity began to decrease. This is also consistent with the reduction of the dissociated free ions as evidenced by the FT-IR result.

As shown in Fig. 6, the ionic conductivities of CPE-x all increased with the increase in the temperature range measured. The linear plots reveal that the ionic conductivity data also follow the Arrhenius equation, $\sigma(T) = \sigma^0 \exp\{-E_a/RT\}$. This is different from what is usually observed for most of the traditional amorphous solid polymer electrolytes, in which the ion conduction follows the VTF equation and the conduction mechanism is believed to involve the segmental motion of the polymer [35]. This also supports that the ion transport in CPE system involves not just the segmental movement of the polymer chains. The E_a values calculated from the Arrhenius plots are listed in Table 2, showing that the activation energy was increased by increasing the ALA–MMT content. This is attributed to the presence of the interaction between the Li^+ ion and the clay in the CPE system. This interaction makes the activation of the Li^+ ion movement more difficult while providing the sites to assist the Li^+ ions to move by the hopping method, thus enhancing the conductivity [36].

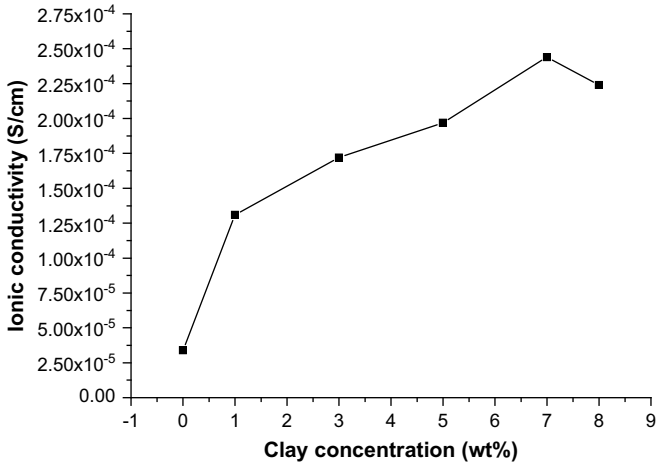

Fig. 5. Relationship of ionic conductivity of the CPE vs. ALA–MMT concentration.

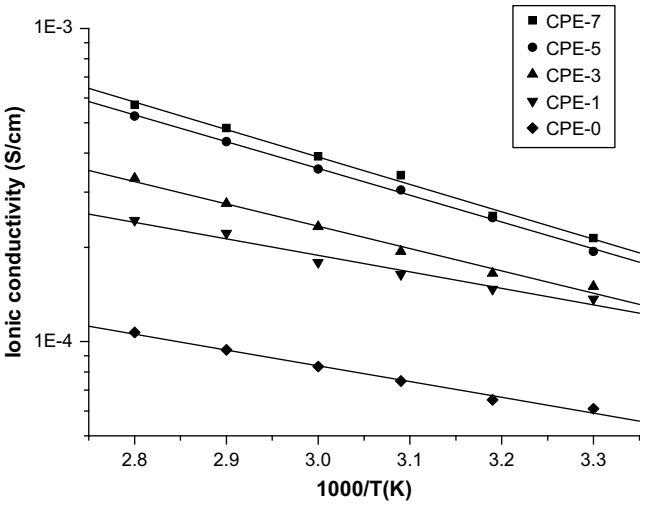

Fig. 6. Arrhenius plots of ionic conductivities of CPE-x.

3.5. Morphology property

Fig. 7 shows the SEM micrographs of the fractured surfaces of PAN and CPE-7 nanocomposites. As shown in Fig. 7(a), the cleavage surface of the PAN membrane shows fractured flakes and straight cleavage border as indicated by the arrows, indicating that the PAN membrane is brittle. On the other hand, Fig. 7(b) shows that the fractured surface of CPE-7 was rough and without fractured flakes. Besides, the interfaces between the clay and the polymer matrix were not visible. This reveals that CPE-7 was not brittle and the ALA–MMT particles were well distributed in the polymer matrix such that the resistance to fracture was enhanced.

3.6. Mechanical property

With the improvement in ionic conductivity through the addition of the clay, preserving the mechanical strength and stability of the electrode/electrolyte interface is important for the CPE as well. However, for most of the polymer electrolytes, an enhancement of conductivity usually leads to a reduction of the mechanical stability and vice versa [26]. Therefore, few mechanical property data of the highly conductive polymer electrolytes have been reported. Nevertheless, the PAN-based composite polymer electrolyte membranes prepared in this study were strong enough and their mechanical properties could be measured. As listed in Table 5, although the pure PAN had high-yield stress, high-tangent modulus and low-yield elongation, exhibiting as a tough film, with the addition of the lithium salt, the yield stress and yield elongation of CPE-0 became rather low. Nevertheless, it is seen that by increasing the content of ALA–MMT, the yield stress and yield elongation of CPE were increased accordingly. For CPE-7, about 100% and 120% increments are found for the yield stress and yield elongation, respectively. The result suggests that the mechanical property of the as-prepared CPE-X was significantly enhanced owing to the

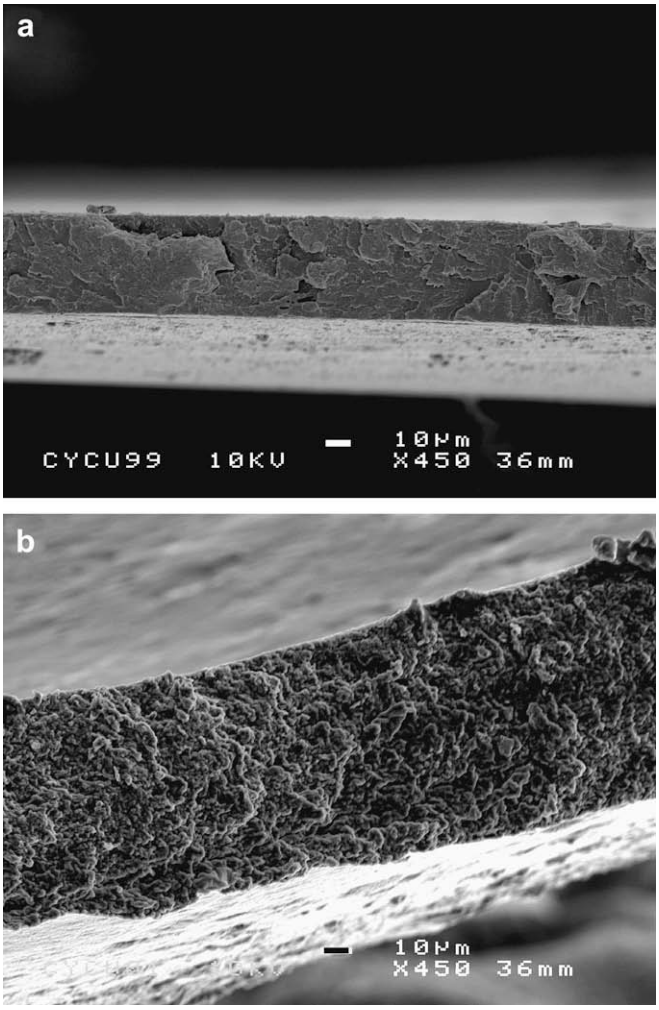

Fig. 7. Fracture surface SEM images of (a) PAN (b) CPE-7.

presence of the well-dispersed ALA–MMT particles. This also indicates that the as-prepared ALA–MMT-containing CPE membranes are more suitable for use as a separator in batteries and pliable to form a conforming interface with the electrodes than that without ALA–MMT.

3.7. Electrochemical stability

The electrochemical stability of the composite polymer electrolyte films was studied by the linear sweep voltammetry and cyclic voltammetry analyses. As can be seen from the linear sweep voltammograms in Fig. 8, for CPE-0, several small current peaks are observed in the low voltage, implying that the CPE without clay was not very stable below 4.25 V, the breakdown voltage. However, no current peak is found through the working electrode from open

Table 5
Mechanical properties of PAN and the CPEs.

Sample	Yield stress (kg cm^{-2})	Yield elongation (%)	Tangent modulus (kg cm^{-2})
PAN	150	1	16,532
CPE-0	16	141	15.0
CPE-1	24	203	15.6
CPE-3	29	240	16.6
CPE-5	32	248	16.5
CPE-7	32	279	23.0

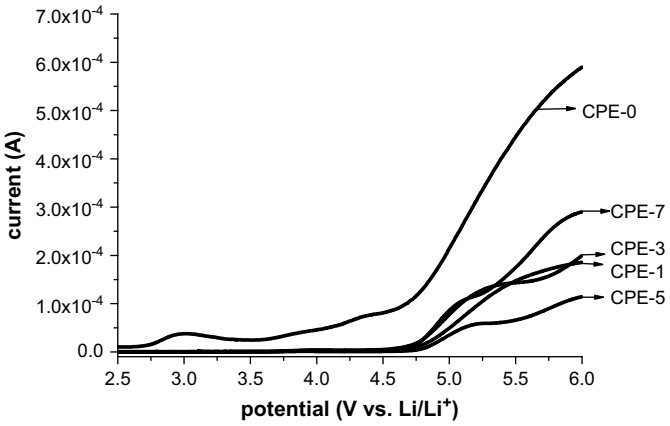

Fig. 8. Linear sweep voltammograms of CPE-x.

circuit potential to 4.75 V for all the CPEs. This reveals that the voltage breakdown of all the as-prepared ALA–MMT-containing CPEs, which were regarded as the potential reasons for the decomposition of electrolytes owing to the oxidation of the anions, was 4.75 V, indicating that the PAN/$LiClO_4$ polymer electrolyte was electrochemically stabilized up to 4.75 V by the addition of the organoclay. This implies that all the ALA–MMT-containing CPEs had a higher anodic stability than CPE-0 and met the requirement for application in lithium polymer battery.

In addition, the electrochemical stability of CPE-7 was further investigated by cyclic voltammetry analysis between 0 V and 4 V. Clearly, the cycling behavior of a cell demonstrates the kinetics of the lithium deposition–stripping process. Fig. 9 shows that the potential for Li stripping indicated by the anodic peak is at 2.2 V vs. Li/Li^+ (oxidation process) and that for the deposition on Pt indicated by the cathodic peak is at 1.7 V vs. Li/Li^+ (reduction process). It shows that the lithium deposition–stripping process is quite efficient. Furthermore, a noteworthy feature found is that the cell swept after 50 cycles still had obvious anodic and cathodic peaks, confirming that CPE-7 had excellent electrochemical stability and cyclability over the potential range between 0 V and 4 V vs. Li/Li^+.

3.8. Lithium ion transference numbers

The cation transference number of an electrolyte, t_+, is defined as the net number of faradays of charge carried across the reference plane by the cationic species in the direction of the cathode, during

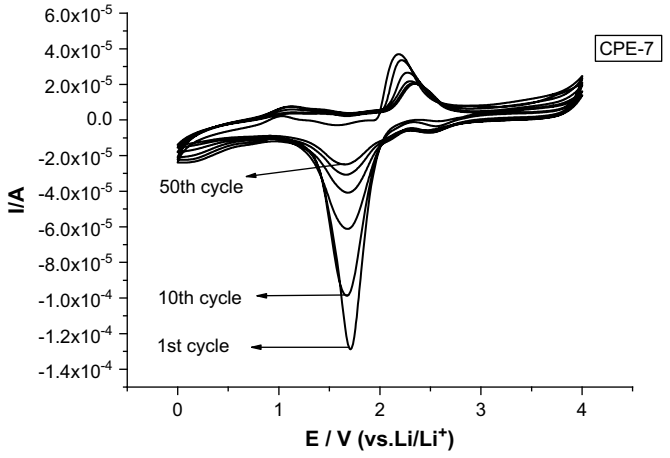

Fig. 9. Cyclic voltammograms of CPE-7 for 50 cycles.

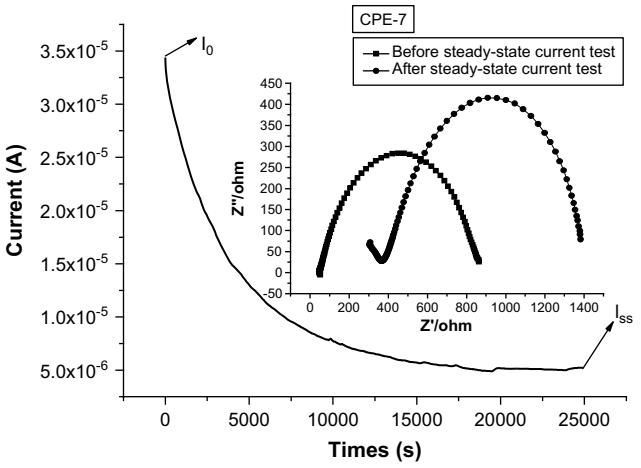

Fig. 10. Current response of Li/CPE-7/Li cell under a dc voltage as a function of time. The inset shows the initial and steady-state impedance response of the cell.

Table 6
Cation transference numbers of CPE-7 and CPE-0 at room temperature.

Sample	I_0 (μA)	I_s (μA)	t_+
CPE-0	24.4	3.70	0.01
CPE-7	34.3	5.23	0.12

the passage of one faraday of charge across the plane. Therefore, it is used to evaluate the contribution of the cationic species to the overall conductivity of the polymer electrolyte. The current vs. time plot measured for t_+ of CPE-7 is shown in Fig. 10 as an example. The corresponding t_+ was calculated using the following equation [28,29]:

$$t_+ = I_s(\Delta V - I_0R_0)/I_0(\Delta V - I_sR_s)$$

I_0: initial current
I_s: steady-state current
R_0: initial interfacial resistance
R_s: steady-state interfacial resistance
ΔV: dc voltage applied

The original data of the electrochemical measurements of the Li/CPE/Li cells with CPE-0 and CPE-7 are summarized in Table 6. As shown, the t_+ value of CPE-0 is very small, but it increased to 0.12 for CPE-7, indicating that with the presence of ALA–MMT, the net number of Li^+ across the direction of the cathode in the CPE significantly increased. This may be attributed to the increase of fraction of the free Li^+ ions caused by the decrease of the interaction between Li^+ and the C≡N groups of the PAN matrix owing to the addition of the ALA–MMT as evidenced by the FT-IR spectrum discussed above. Nevertheless, this value of t_+ is still lower than that reported previously [26]. This may be attributed to the barrier caused by the platelet type of clay.

4. Conclusion

This study demonstrated that dispersing the 12-amino-dodecanoic acid ($NH_2(CH_2)_{11}COOH$) modified clay (ALA–MMT) into the PAN/$LiClO_4$ polymer electrolyte made the composite a better polymer electrolyte than that without the clay. The results showed that with the addition of ALA–MMT, the interaction of Li^+ and C≡N was reduced and the Li^+ cations were less constrained in the polymer matrix and moved more freely in the polymer electrolytes. Besides, the ALA–MMT clay allowed the lithium salt to dissolve in the PAN matrix, resulting in the increase of the concentration of the solvated Li^+. Therefore, the ionic conductivity of the as-prepared ALA–MMT-containing polymer electrolyte was enhanced. The ionic conductivity of the PAN/$LiClO_4$/ALA–MMT nanocomposite polymer electrolyte was increased seven-fold when 7 wt% of ALA–MMT was added to the composite. The lithium transference number of the polymer electrolyte was also significantly increased with the addition of ALA–MMT. Besides, the results of the voltammetry measurements showed that the anodic and cathodic peaks were well maintained after 50 cycles, confirming that the as-prepared CPE had excellent electrochemical stability and cyclability over the potential range between 0 V and 4 V vs. Li/Li^+.

Acknowledgments

The authors would like to thank Chung Yuan Christian University, Taiwan (CYCU-95-CR-C) and the National Science Council (NSC 94-2113-M-033-010) of the Republic of China for providing financial support to this research.

References

[1] Stephan AM, Nahm KS. Polymer 2006;47:5952.
[2] Zhang SS. J Power Sources 2007;164:351.
[3] Wang M, Dong S. J Power Sources 2007;170:425.
[4] Ho Joo Jae, Chan Bae Young. Polymer 2006;47:7153.
[5] Wu I-Der, Chang Feng-Chih. Polymer 2007;48:989.
[6] Xi J, Qiu X, Cui M, Tang X, Zhu W, Chen L. J Power Sources 2006;156:581.
[7] Kim JW, Ji KS, Lee JP, Park JW. J Power Sources 2003;119–121:415.
[8] Xi J, Qiu X, Zheng S, Tang X. Polymer 2005;46:5702.
[9] Shahzada Ahmad, Bohidar HB, Sharif Ahmad, Agnihotry SA. Polymer 2006;47:3583.
[10] Chen HW, Chang FC. J Polym Sci Part B Polym Phys 2001;39:2407.
[11] Loyens W, Maurer FHJ, Jannasch P. Polymer 2005;46:7334.
[12] Wang WS, Chen HS, Wu YW, Tsai TY, Chen-Yang YW. Polymer 2008;49:4826.
[13] Kawasumi M, Hasegawa N, Kato M, Usuki A, Okada A. Macromolecules 1997;30:6333.
[14] Yeh JM, Liou SJ, Lin CY, Cheng CY, Chang YW, Lee KR. Chem Mater 2002;14:154.
[15] Chen HW, Lin TP, Chang FC. Polymer 2002;43:5281.
[16] Hwang JJ, Liu HJ. Macromolecules 2002;35:7314.
[17] Thakur AK, Pradhan DK, Samantaray BK, Choudhary RNP. J Power Sources 2006;159:272.
[18] Nan CW, Fan L, Lin Y, Cai Q. Phys Rev Lett 2003;91(1–4):266104.
[19] Kao HM, Tsai YY, Chao SW. Solid State Ionics 2005;176:1261.
[20] Reddy MJ, Chu PP. J Power Sources 2004;135:1.
[21] Tominaga Y, Asai S, Sumita M, Panero S, Scrosati B. J Power Sources 2005;146:402.
[22] Xia J, Qiua X, Zhua W, Tang X. Microporous Mesoporous Mater 2006;88:1.
[23] Chen-Yang YW, Wang YL, Chen YT, Li YK, Chen HC, Chiu HY. J Power Sources 2008;182:340.
[24] Ngyen QT, Baird DG. Adv Polym Tech 2006;25(4):270.
[25] Yeh JM, Chen CL, Chen YC, Ma CY, Lee KR, Wei Y, et al. Polymer 2002;43:2729.
[26] Chen-Yang YW, Chen HC, Lin FJ, Chen CC. Solid State Ionics 2002;150:327.
[27] Chen-Yang YW, Lee YK, Chen YT, Wu JC. Polymer 2007;48(10):2969.
[28] Bruce PG, Vincent CA. J Electroanal Chem 1987;225:1.
[29] Evans J, Vincent CA, Bruce PG. Polymer 1987;28:2324.
[30] Wieczorek W, Zalewska A, Raducha D, Florjan'czyk Z, Stevens JR. J Phys Chem B 1998;102:352.
[31] Salomon M, Xu M, Eyring EM, Petrucci S. J Phys Chem 1994;98:8234.
[32] Wieczorek W, Lipka P, Zukowska G, Wycislik H. J Phys Chem B 1998;102:6968.
[33] Wang XL, Fan LZ, Mei A, Ma FY, Lin YH, Nan CW. Electrochim Acta 2008;53:2448.
[34] Huang B, Wang Z, Chen L, Xue R, Wang F. Solid State Ionics 1996;91:279.
[35] Forsyth M, Sun Ji, MacFarlance DR. Solid State Ionics 1998;112:161.
[36] Capiglia C, Yang J, Imanishi N, Hirano A, Takeda Y, Yamamoto O. Solid State Ionics 2002:154.